Chapter 1

NV-NV CR under transverse or low fields: application to magnetometry

(mentionner l'article ici !).... The main motivation for this study was the potential to use NV-NV CR as a low field magnetometry protocol. Indeed, while NV-NV CR lines can be used to perform magnetometry with non zero fields [les russes], there are several advantages to use NV-NV CR as close to the zero magnetic field region, in particular the non dependence of the magnetic field orientation with respect to the crystal lattice. The behavior of

1.1 NV spin Hamiltonian under low and transverse fields

Before looking at the NV-NV CR in the low or transverse field regime, we first need to consider how the general NV physics is modified under those regimes, and in particular we need to look at the modifications of the spin Hamiltonian and the change in the eigenstates.

1.1.1 NV spin Hamiltonian in zero external magnetic field

In the absence of external magnetic field, we have to take into account other elements which would otherwise be of second order in the spin Hamiltonian. These elements are: the random local magnetic fields caused by paramagnetic impurities, the local electric field caused by charged impurities, and the crystal strain [1–3]. The hyperfine splitting due to nearby nuclei will be considered separately, although to a large extent it behaves like a local magnetic field.

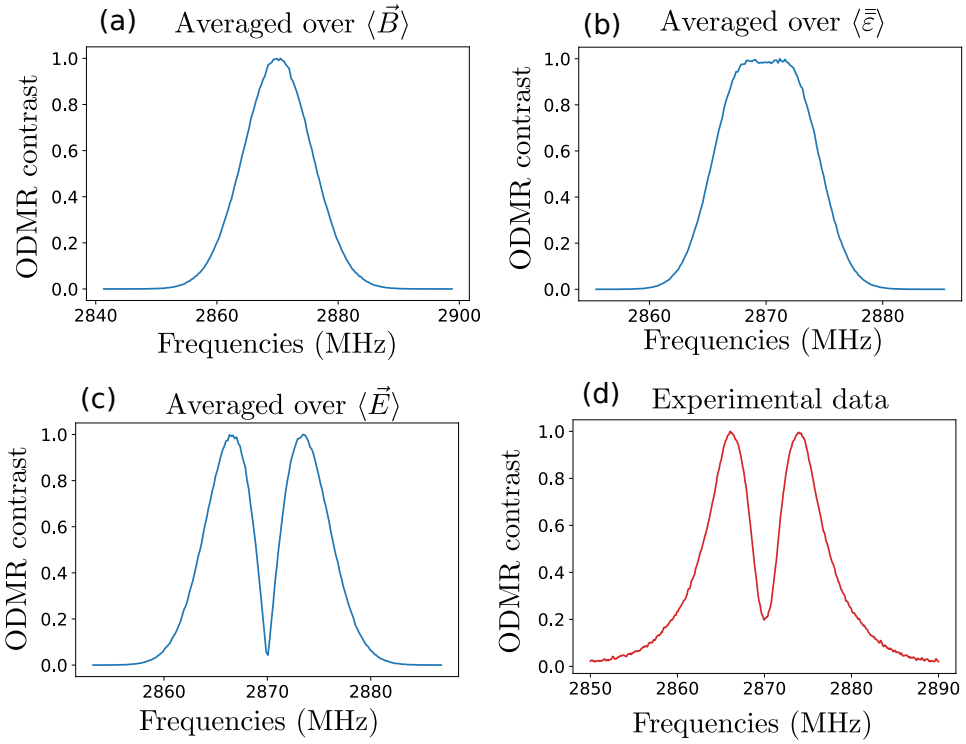

Figure 1.1: Simulations of inhomogeneous zero field ODMR when sampling various parameters. a) Simulation when sampling each components of the magnetic field over a Gaussian of deviation $\sigma = 2$ G. b) Simulation when sampling each components of the strain tensor $\bar{\bar{\varepsilon}}$ over a Gaussian of deviation $\sigma = 2 \cdot 10^{-4}$. c) Simulation when sampling each components of the electric field over a Gaussian of deviation $\sigma = 2 \cdot 10^5$ V/cm. d) Experimental ODMR spectrum in zero external field taken on sample ADM-150-2

Due to the large zero field splitting $D = 2870MHz$ between the $|0\rangle$ and $|\pm 1\rangle$ states, we will consider the $|0\rangle$ to always be an eigenstate of the spin Hamiltonian under zero external field (which is equivalent to say that we neglect the terms in $|0\rangle \langle \pm 1|$ in the spin Hamiltonian). The problem is then reduced to the $\{|-1\rangle, |+1\rangle\}$ subsystem.

The NV^-spin Hamiltonian in the $\{|-1\rangle, |+1\rangle\}$ basis can be written as [2]:

$$\mathcal{H} = \begin{pmatrix} D - \gamma_e B_\parallel + f_\parallel(\mathbf{E}) + g_\parallel(\bar{\bar{\varepsilon}}) & f_\perp(\mathbf{E}) + g_\perp(\bar{\bar{\varepsilon}}) \\ f_\perp^*(\mathbf{E}) + g_\perp^*(\bar{\bar{\varepsilon}}) & D + \gamma_e B_\parallel + f_\parallel(\mathbf{E}) + g_\parallel(\bar{\bar{\varepsilon}}) \end{pmatrix}, \tag{1.1}$$

where $B_\parallel$ is the component of the magnetic field along the NV axis, and $f_\parallel, f_\perp, g_\perp$, and $g_\parallel$ are functions of the electric field $\mathbf{E}$ and the strain tensor $\bar{\bar{\varepsilon}}$, whose expressions are:

$$f_{\parallel}(\mathbf{E}) = d_{\parallel} E_z, \tag{1.2}$$

$$f_{\perp}(\mathbf{E}) = d_{\perp}(E_x + iE_y), \tag{1.3}$$

$$g_{\parallel}(\bar{\bar{\varepsilon}}) = h_{41}(\varepsilon_{xx} + \varepsilon_{yy}) + h_{43}\varepsilon_{zz}, \tag{1.4}$$

$$g_{\perp}(\bar{\bar{\varepsilon}}) = \frac{1}{2}\left[h_{16}(\varepsilon_{zx} + i\varepsilon_{zy}) + h_{15}\left(\frac{\varepsilon_{yy} - \varepsilon_{xx}}{2} + i\varepsilon_{xy}\right)\right], \tag{1.5}$$

where $d_{\parallel} = 0.35$ Hz cm/V and $d_{\perp} = 17$ Hz cm/V have been measured experimentally [4], and $h_{43} = 2300$ MHz, $h_{41} = -6420$ MHz, $h_{15} = 5700$ MHz and $h_{16} = 19660$ MHz were computed through DFT [2] and show reasonable agreement with experiments [5].

Importantly, as pointed in [3] we notice that both the electric field and the strain have a *shifting* component ($f_{\parallel}$ and $g_{\parallel}$) which shifts equally both eigenstates of the Hamiltonian, and a *splitting* component ($f_{\perp}$ and $g_{\perp}$) which splits in energy the two eigenstates.

The main difference between the electric field and the strain is in the numerical prefactors of these components: for the electric field, the splitting parameter $d_{\perp}$ is ~ 50 times higher than the shifting parameter $d_{\parallel}$, which will result on average to a strong energy split without much shifting. For the strain however, the splitting parameters h_{15} and h_{16} are only ~ 3 times higher than the shifting parameters h_{43} and h_{41}. The shift in energy will therefore tend to blur the energy split when averaging over a large number of spins.

Fig. 1.1 shows a simulation of how each parameters of the spin Hamiltonian - local magnetic field, local electric field and strain - affects the zero external field ODMR profile. To do these simulations, I sampled each parameters separately 10^6 times and plotted the histogram of the two eigenvalues of the Hamiltonian written in eq. 1.1. Fig. 1.1-d) shows an experimental zero field ODMR spectrum, typical of what we observe with dense NV ensembles.

Experimentally, almost all our samples show the characteristic two bumps in zero external field ODMR. Given the simulation results, the only parameter that can give rise to this shape is the electric field. We will therefore consider that the NV Hamiltonian of our samples is dominated by the local electric field, and more specifically by the transverse electric field $E_{\perp} \equiv E_x + iE_y$ given the ratio between $d_{\perp}$ and $d_{\parallel}$.

We will then adopt the following simplified Hamiltonian for the zero external field regime:

$$\mathcal{H} = \begin{pmatrix} D & 0 & d_{\perp}E_{\perp}^{*} \\ 0 & 0 & 0 \\ d_{\perp}E_{\perp} & 0 & D \end{pmatrix}, \tag{1.6}$$

whose eigenvectors are $|0\rangle$ and$|\pm\rangle$ of eigenvalues 0 and $D \pm d_\perp|E_\perp|$, where $|\pm\rangle$ are defined as:

$$|\pm\rangle = \frac{|+1\rangle \pm e^{-i\phi_E}|-1\rangle}{\sqrt{2}}, \tag{1.7}$$

where $\tan(\phi_E) = E_y/E_x$.

1.1.2 NV spin Hamiltonian under purely transverse magnetic field

We will consider here the case of purely transverse magnetic field with respect to the NV axis, i.e. $\mathbf{B} = B_x\hat{e}_x + B_y\hat{e}_y$, and more specifically the regime where $d_\perp E_\perp < \frac{(\gamma_e B_\perp)^2}{D} << D$. In practice, this generally means 20 G $\lesssim$ B$_\perp$ $\lesssim$ 200 G.

In this regime, the NV Hamiltonian eigenstates are similar to the case dominated by the transverse electric field and can be written $\approx |0\rangle, |\pm\rangle$[6, 7], of eigenvalues $\approx -\frac{(\gamma_e B_\perp)^2}{D}, D$ and $D + \frac{(\gamma_e B_\perp)^2}{D}$, where:

$$|\pm\rangle = \frac{|+1\rangle \pm e^{-2i\phi_B}|-1\rangle}{\sqrt{2}}, \tag{1.8}$$

and $\tan(\phi_B) = B_y/B_x$.

For the case where $d_\perp E_\perp \sim \frac{(\gamma_e B_\perp)^2}{D}$ and $\phi_E \neq 2\phi_B$, the eigenstates of the Hamiltonian are still $|0\rangle, |\pm\rangle$ with a relative angle ϕ in between ϕ_E and $2\phi_B$.

In conclusion, whenever the spin Hamiltonian is dominated by a transverse field, either electric or magnetic, we can consider that the eigenstates of the spin Hamiltonian or $|0\rangle, |-\rangle$ and $|+\rangle$, whereas when the Hamiltonian is dominated by the longitudinal magnetic field, its eigenstates are $|0\rangle, |-1\rangle$ and $|+1\rangle$.

1.1.3 Hyperfine coupling and inhomogeneous broadening

We will now look at the modification in the ODMR linewidths caused by the different magnetic field regimes. These change are relevant to our study of NV-NV CR due to the relation between the dipole-induced relaxation rate and T_2^* detailed in sec. [REF].

A consequence of the change in the Hamiltonian eigenstates from the $\{|0\rangle, |\pm1\rangle\}$ to the $\{|0\rangle, |\pm\rangle\}$ basis is that the Hamiltonian eigenvalues are sensitive to different part of the environment. In the $\{|0\rangle, |\pm1\rangle\}$, the eigen energies are linearly sensitive to (longitudinal) magnetic field, and only sensitive to electric fields at the second order, and vice versa for the $\{|0\rangle, |\pm\rangle\}$ basis.

These different sensitivities affect both the inhomogeneous broadening, due to the local electric and magnetic noise, and the hyper-fine coupling

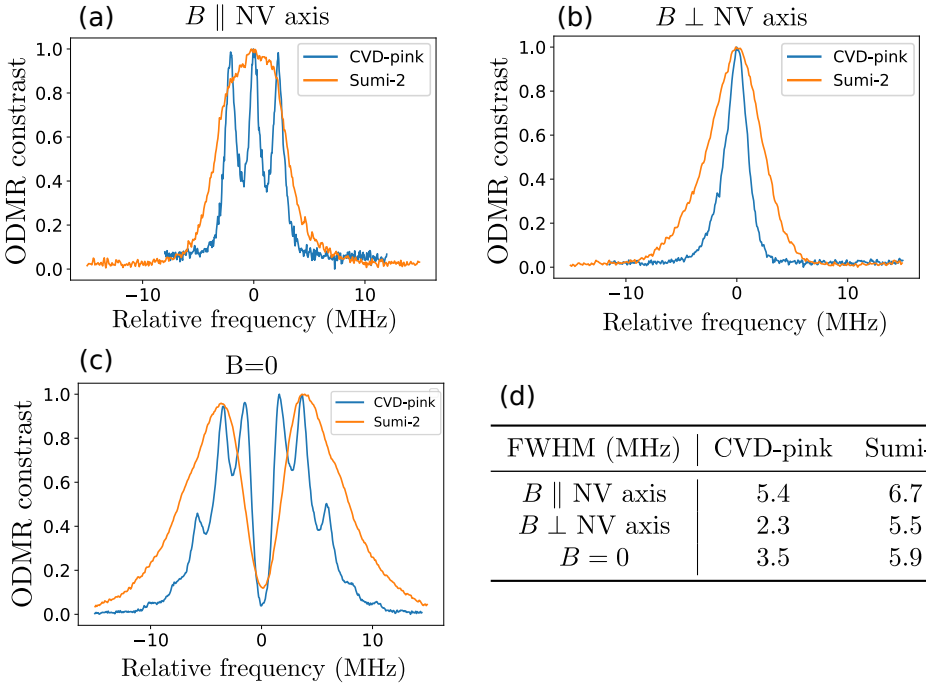

(d)

FWHM (MHz)	CVD-pink	Sumi-2
$B \parallel$ NV axis	5.4	6.7
$B \perp$ NV axis	2.3	5.5
$B = 0$	3.5	5.9

Figure 1.2: tata. Changer les T1 avec T1ph=5ms

to the various surrounding nuclei. These effects can drastically modify the ODMR lineshape in zero external magnetic field [8] or purely transverse magnetic field [6, 7].

We will only consider here the hyper-fine splitting caused by the ^{14}N nuclei of the nitrogen atom forming the NV center. ^{14}N represents 99.6 % of natural abundance nitrogen atoms, and it has an $I = 1$ nuclear spin. The full 3×3 Hamiltonian of the NV center in these conditions can be written:

$$\mathcal{H} = \mathcal{H}_e + \mathcal{H}_n + \mathbf{S}\bar{\bar{A}}\mathbf{I}, \tag{1.9}$$

where $\mathbf{S}$ is the electronic spin operator, $\mathbf{I}$ the nuclear spin operator, $\mathcal{H}_e$ the previously described electronic spin Hamiltonian, $\mathcal{H}_n$ the nuclear spin Hamiltonian and $\bar{\bar{A}}$ the hyper fine tensor. $\mathcal{H}_n$ and $\bar{\bar{A}}$ can be written:

$$\bar{\bar{A}} = \begin{pmatrix} A_{xx} & 0 & 0 \\ 0 & A_{yy} & 0 \\ 0 & 0 & A_{zz} \end{pmatrix} \tag{1.10}$$

$$\mathcal{H}_n = \gamma_N \mathbf{I} \cdot \mathbf{B} + Q I_z^2, \tag{1.11}$$

where $\gamma_N = 0.308$ kHz/G, $Q = -4.945$ MHz, $A_{zz} = -2.162$ MHz and $A_{xx} = A_{yy} = -2.62$ MHz [9].

Fig. 1.2 shows ODMR spectra for two samples, CVD-pink and Sumi-2, in three magnetic configuration: for a strong longitudinal magnetic field, where the NV eigenbasis is $\{|0\rangle, |\pm1\rangle\}$, and for a strong transverse magnetic field or no magnetic field, where the NV eigenbasis is $\{|0\rangle, |\pm\rangle\}$. A table with the full width at half maximum of each ODMR line is shown in Fig. 1.2-d)

While both samples are relatively equivalent in term of NV concentration ([NV]=3 $\sim$ 5 ppm), sample Sumi-2, being a Type 1B HPHT sample, contains significantly more impurities besides NV centers, most likely P1 centers. These impurities cause both magnetic (because of paramagnetic impurities) and electric (because of charged impurities) field noise.

Fig. 1.2-a) allows us to evaluate the magnetic field noise in both samples, since the $|\pm1\rangle$ states are not sensitive to weak electric fields. We indeed find that the Sumi-2 sample has much more magnetic noise, to the point where the hyper-fine structure is no longer resolved. The total width of the line however is mostly dominated by the hyper-fine splitting, which result in a similar total linewidth in both cases

We should note that the current practice in magnetometry is to consider only of the three hyper-fine lines when they are resolved. This is because magnetometry protocol usually relies on a microwave field with a very well defined frequency, which can effectively select only one of the lines. In our case however, we have to consider the spectral overlap between NV centers and fluctuators, which have an additional broadening of $2\gamma_f \approx 6$ MHz [REF] that completely obscures the hyper-fine structure. We therefore have to consider the full linewidth, even when the hyper-fine structure is resolved.

Fig. 1.2-b) allows us to evaluate the electric field noise in both samples, since the $|\pm\rangle$ states are not sensitive to weak magnetic fields. Similarly, the hyper-fine structure is hidden in this configuration since all three hyper-fine levels are nearly-degenerate, provided that $\frac{(\gamma_e B_\perp)^2}{D} > A_{xx}, A_{zz}, Q$ which is typically the case for $B_\perp > 40$ G. We can note that the electric field noise is significantly stronger in the HPHT sample, which leads to an ODMR linewidth more than twice as big.

Finally, 1.2-c) shows the linewidth of both samples for zero external magnetic field. For sample Sumi-2, the profile and linewidth is similar to the case of the purely transverse magnetic field, which is consistent with the fact that the electric field noise is stronger than the residual magnetic fields (earth magnetic field and hyper-fine interaction). For sample CVD-pink however, the electric field noise is smaller than the hyper-fine interaction, meaning that only the $|m_I = 0\rangle$ states (the ones closest to the central dip) will be dominated by the electronic noise, and be in the electronic states $|m_e = \pm\rangle$. The $|m_I = \pm1\rangle$ states are dominated by the hyper-fine field and are in the electronic $|m_e = \pm1\rangle$ basis.

Overall, we are mostly interested in the linewidth of the ODMR lines

for various magnetic field conditions. While these linewidth are quite significantly changed for sample CVD-pink, the change is less pronounced on sample Sumi-2. Most HPHT samples we used are from type 1B diamond, and behave similarly to sample Sumi-2. Since almost all measurements in this chapter will be conducted on HPHT samples, we will consider the modification of T_2^* as a minor effect.

1.2 NV-NV CR in the low magnetic field regime

In this part, we will study the cross-relaxation between NV centers under low magnetic field, whose spin Hamiltonian is dominated by a transverse electric field. Understanding the various mechanisms operating in this regime will be important for the magnetometry protocol presented after.

1.2.1 Experimental observations

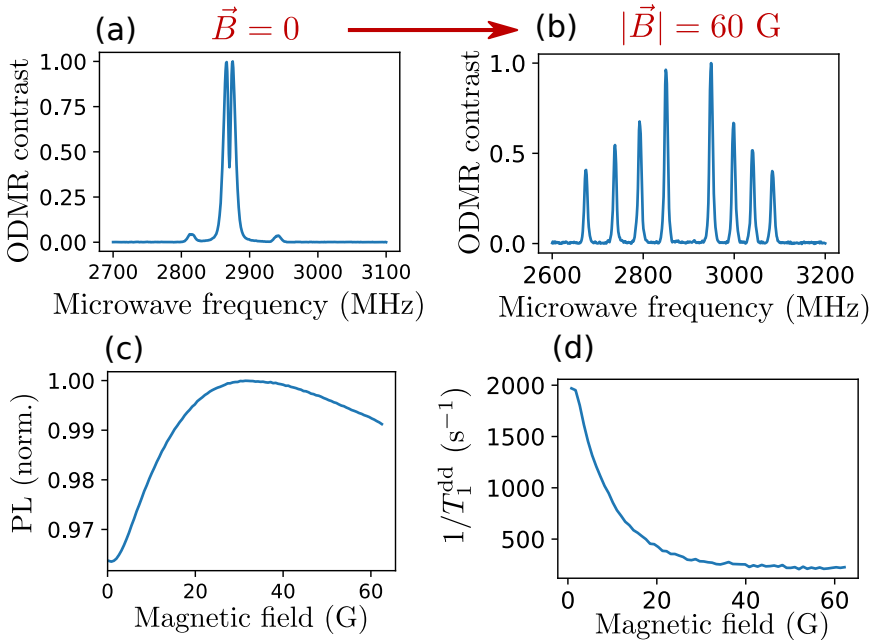

Figure 1.3: tata. Changer les T1 avec T1ph=5ms

We will start by showing that NV-NV CR behaves differently in the low magnetic field regime compared to the longitudinal field dominated regime which we studied in the last chapter.

The main issue with studying NV-NV CR in low to zero magnetic field is that there are many competing effects happening simultaneously, with few buttons to adjust to isolate each effects.

Fig. 1.3-c) and d) show the evolution of the NV PL and stretched lifetime T_1^{dd}, defined in the last chapter [REF], as the magnetic field is scanned from 0 to 60 G. The ODMR at the initial and final magnetic fields are shown in Fig. 1.3-a) and b).

While it is clear that the spin lifetime as well as the PL increases with the magnetic field, there is no clear indication that this is because of the specificity of the low field region. Indeed, the most likely explanation in this case is that the four classes of NV centers get split apart as the magnetic field increases, which reduces the density of resonant fluctuators for each NV centers.

We can note however that the PL is not an exact mirror of the spin dynamics: while the low field drop in PL is indeed associated with a reduced spin lifetime, the drop in PL at higher magnetic field comes from the states mixing induced by the transverse magnetic field, and is not associated with a modification of the spin dynamics (to the first order).

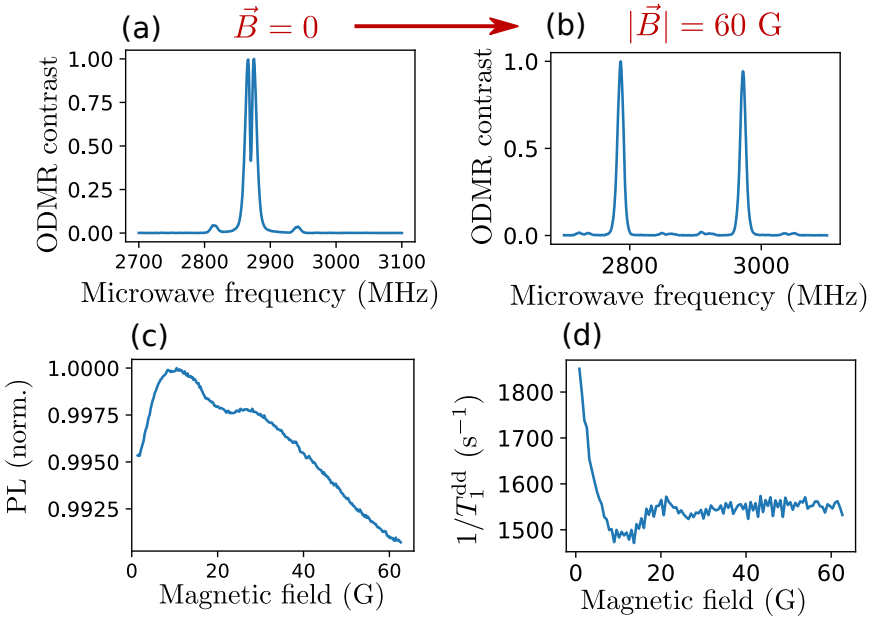

Figure 1.4: Same measurements as Fig. 1.3, still on sample ADM-150-1, but with **B** along the [100] axis. Changer les T1 avec T1ph=5ms

Fig. 1.4 presents a way to circumvent this issue: by applying the magnetic field along the [100] crystalline axis, we can make sure that the four classes of NV centers always stay resonant regardless of the magnetic field amplitude.

We can notice that there still is a decrease of both the PL and T_1^{dd} in low field, although considerably smaller than the previous case: in Fig. 1.3, T_1^{dd} was reduced by a factor of [REF] in zero field, whereas in Fig. 1.4, it

was only reduced by a factor of [REF]. The main reason for the PL and T_1 drop was indeed the co-resonance between the four classes.

Nevertheless, the fact that there is a drop in zero field when $\mathbf{B} \parallel [100]$ cannot be explained by considering only the inter-class resonances. There are some additional depolarization mechanisms which are proper to the zero field region. We should also note that, while the zero-field PL contrast is bigger in Fig. 1.3-c) than in Fig. 1.4-c), the PL slope, which is the limiting factor for sensing ability, is actually very similar in both cases with a value $\sim [REF]$ G^{-1}.

We can also note a drop in PL and a corresponding increase of $1/T_1^{\mathrm{dd}}$ for $B \sim 20$ G which corresponds to the NV$-^{13}$C-NV cross-relaxation discussed in [REF]

1.2.2 Potential causes for low field depolarization

We will discuss here three possible reasons for the zero field depolarization observed in Fig. 1.4. Once presented, we will try to hierarchized the contribution of each of these effects.

Eigenstates modification

The first explanation is the modification of the dipole-dipole interaction caused by the change of the NV Hamiltonian eigenbasis from $\{|0\rangle, |\pm1\rangle\}$ when $\mathbf{B} \neq 0$ to $\{|0\rangle, |\pm\rangle\}$ when $\mathbf{B} = 0$.

This modification arise from the new form of the dipole-dipole Hamiltonian in the $\{|0\rangle, |+\rangle, |-\rangle\} \times \{|0\rangle, |+\rangle, |-\rangle\}$ basis. We justify this change of basis, where we only considered the single NV Hamiltonian instead of the full two-spins Hamiltonian, by the fact that we are in the weak coupling regime, where $\langle \mathcal{H}_{dd} \rangle \approx 50$ kHz $\ll \frac{1}{2\pi \mathrm{T}_2^*} \approx 5$ MHz meaning that we can treat the dipole-dipole interaction perturbatively. To compute the decay rate with these new eigenstates, we now need to consider the $\langle 0, \pm|\mathcal{H}_{dd}|\pm, 0\rangle$ matrix elements instead of the $\langle 0, \pm1|\mathcal{H}_{dd}|\pm1, 0\rangle$ ones.

The computation of the decay rates in the new eigenbasis involve the averaging of these matrix elements which is detailed in appendix [REF]. The computation in this case is complicated by the fact that the transverse field (either $\mathbf{E}$ or $\mathbf{B}$) responsible for the splitting of the $|\pm\rangle$ levels breaks the Hamiltonian symmetry in the (xy) plane. This means that the dipole-dipole coupling between two spins will depend on their relative x and y axis, defined by the local transverse field, on top of the relative z axis defined by the NV axis.

We therefore need to make an assumption on the distribution of the transverse field in the sample. In zero external magnetic field where the dominant transverse field comes from randomly spaced charged impurities, we can expect the x and y axes to be randomly sampled in their respective

(xy) plane. However, since the NV-fluctuator CR is dominated by the closest neighbor of each spin (due to the $1/r^6$ scaling in eq. [REF]), there could still be local correlations in the transverse field felt by the NV and its nearest fluctuator.

We then computed the decay rates for the two extreme cases: first, we consider that the x and y axis of each spin is randomly sampled, which correspond to a correlation length of the transverse field $l_c = 0$, and secondly we considered the case where the dominant transverse field as a fixed orientation in the whole sample corresponding to $l_c = \infty$.

We found for $\mathbf{B} = 0$ that the expected decay rate was $\Gamma_1 = 51.4\Gamma_0^{\text{th}}$ if $l_c = 0$ and $\Gamma_1 = 55.0\Gamma_0^{\text{th}}$ if $l_c = \infty$. Γ_0^{th} has the same definition as in table [REF], it is the expected decay rate for an isolated class in the $\{|0\rangle, |\pm1\rangle\}$ basis.

In both cases, this is a moderate ($\sim 20\%$) increase compared to $\Gamma_1 = 42.8\Gamma_0^{\text{th}}$ which we previously found for $\mathbf{B} \parallel [100]$, where all four classes were degenerate but the Hamiltonian eignebasis was $\{|0\rangle, |\pm1\rangle\}$. The change in the Hamiltonian eigenbasis for low field is therefore a possible candidate to explain the low field depolarization in Fig. 1.4

Double flips

Table 1.1: Simulated depolarization rate for flip-flops and double flips in zero magnetic field

	$l_c = 0$	$l_c = \infty$
$\bar{G}^2 = 1$	$126.8\Gamma_0^{\text{th}}$	$126.8\Gamma_0^{\text{th}}$
$\bar{G}^2 = 0.5$	$NA\Gamma_0^{\text{th}}$	$NA\Gamma_0^{\text{th}}$
$\bar{G}^2 = 0$	$51.4\Gamma_0^{\text{th}}$	$55\Gamma_0^{\text{th}}$

Another effect which happens only at low magnetic field is the possibility of double flip between the NV center and the fluctuator, which is the simultaneous flip of both spins in the same directions, for example going from $|0, -1\rangle$ to $|+1, 0\rangle$. The processes $|0, \pm1\rangle \langle\mp1, 0|$ are resonant for $B = 0$ and not anymore when the degeneracy between the $|\pm1\rangle$ states is lifted by the magnetic field.

We have seen however that for weak magnetic fields the eigenstates of each NV Hamiltonian are $|\pm\rangle$ and not $|\pm1\rangle$, due to the transverse electric field. And the $|+\rangle$ and $|-\rangle$ states are not resonant in zero magnetic field. But we can see from Fig. 1.1-d) or 1.2-c) that the splitting $2d_\perp E_\perp \approx 8$ MHz is of the same order than the $1/T_1^{\text{dd}}$ profile of linewidth $\Gamma^{\text{dd}} \approx 8.8$ MHz measured on Fig. [REF]. In zero external magnetic field, the $|+\rangle$ and $|-\rangle$ states are therefore close enough in energy that double flip can take place.

To compute the depolarization induced by the double flips, we need to

add another decay channel in the fluctuator model, on top of the flip-flop one. We also need to take into account the fact that the $|+\rangle$ and $|-\rangle$ states are not fully resonant, which will modify the $\bar{G}$ factor defined in [REF]. Finally, the question about the correlation length of the electric field also needs to be asked.

The results are summed up in Table 1.1. We again give the results for the two extreme cases regarding the correlations in the electric field, and we show three possible scenario regarding the pseudo-resonance of the $|+\rangle$ and $|-\rangle$ states, represented by the $\bar{G}^2$ factor: $\bar{G}^2 = 1$ means that the states are fully resonant ($\omega_+ - \omega_- \ll \Gamma^{\mathrm{dd}}$), this would be the maximum possible decay rate involving the double flips. $\bar{G}^2 = 0.5$ represents the case where the splitting between the states is equal to the fluctuator linewidth ($\omega_+ - \omega_- \approx \Gamma^{\mathrm{dd}}$). This is close to the the experimental values we have. Finally $\bar{G}^2 = 0$ correspond to the case where the states are too far detuned for the double flips ($\omega_+ - \omega_- \gg \Gamma^{\mathrm{dd}}$). We come back to the results of the last section where only considered the flip-flops.

We therefore predict that the double flips amounts for an increase of the decay rate by [REF] % (taking $\bar{G}^2 = 0.5$) compared to the previous case.

T_2^* modification

The last aspect we considered was the change in T_2^* (we include the change in the hyper-fine interaction in the T_2^*) for weak magnetic field, as discussed in sec. 1.1.3.

To quantify its impact in the depolarization rate, we employ eq. [REF], wherche use the values $2\gamma_f = 6.5$ MHz and we take for $\Gamma_f = \Gamma_N V$ the values of half width at half maximum found in Fig. 1.2.

We then find that the modification of T_2^* should increase the decay rate in zero field by $\sim 6\%$ for sample Sumi-2, and by $\sim 19\%$ for sample CVD-pink.

Summary

Fig. 1.5 recapitulate the various mechanisms at play in the low field depolarization of NV ensemble.

We start from from the simplest case where every classes are sepctrally isolated and the only dipole-induced relaxation coms from the flip-flop between NV and fluctuators from the same class. We then consider the case where all four classes are resonant ($B \parallel [100]$) and finally the case B=0.

The three extra depolarization mechanisms in zero field are then detailed, with the predicted increase of depolarization rate for each step. The predicted rates in zero field depend on several parameters, we chose the following ones to compute the different numerical values: $l_c = 0$, $\bar{G}^2 = 0.5$, $2\gamma_f = 6.5$ MHz and $2/T_2^* = 5.9$ MHz (corresponding to sample Sumi-2 if we assume a Lorentzian ODMR profile).

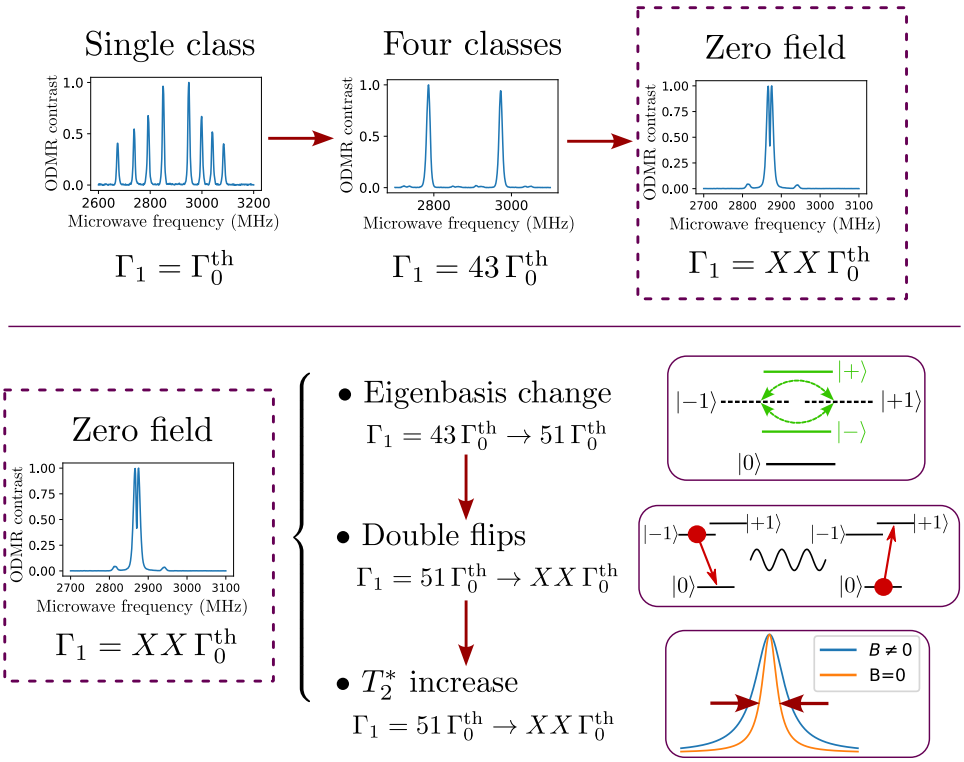

Figure 1.5: Visual summary of the different depolarization effects in low magnetic field and their predicted depolarization rate

1.2.3 Other potential causes

We have also considered two other causes that we have ultimately ruled out in this case.

Magnetic field alignment

The first is a potential misalignment of the magnetic field with the [100] axis, which would cause a splitting of the 4 classes as the magnetic field increases. This hypothesis is not consistent with the observations in Fig. 1.4-d): we would expect a small misalignment to cause a slow but steady decrease of $1/T_1^{\text{dd}}$ as the magnetic field is increased. Instead we observe a sharp decrease followed by a pseudo-plateau.

We still tried to estimate the sensitivity of the low field depolarization with the field orientation. Fig. 1.6 shows PL scans on sample CVD-pink for various alignment of the magnetic field around the [100] axis. We estimate our alignments to be precise within $\pm 1°$. We can see that the central feature is almost unaffected by the orientation within $[-3°{:}+3°]$ which confirms that the low field depolarization does not come from a field misalignment.

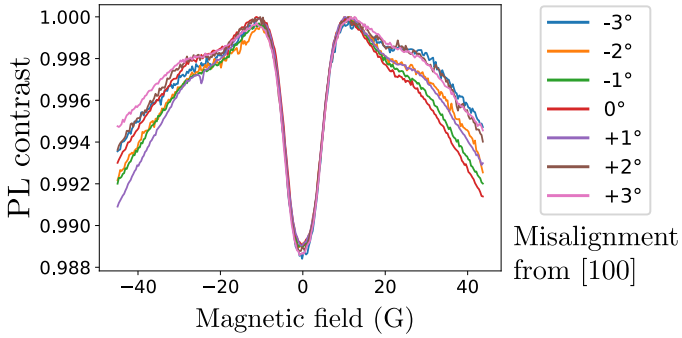

Figure 1.6: PL of sample CVD-pink as a function of the magnetic field for various misalignment of the field direction with the [100] axis

Laser polarization

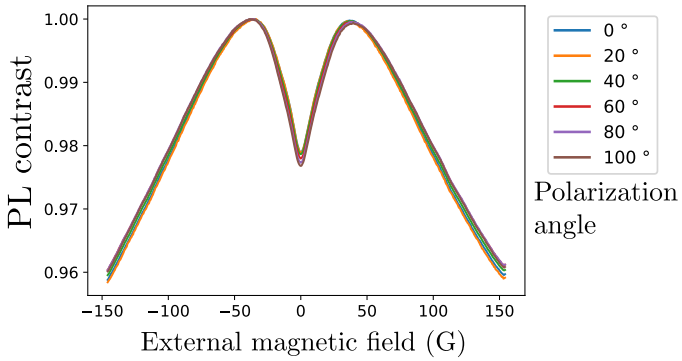

Figure 1.7: tata

Other studies [10, 11] previously saw a correlation between the zero magnetic field PL dip and the polarization angle of the laser with respect to the magnetic field.

Fig. 1.7 shows PL scans on sample ADM-150-3 for various polarization angle of the incident laser. We chose to apply the magnetic field in the laser polarization plane, in a direction that did not match any particular crystalline planes.

We can see no clear differences between the different polarization angles used, whereas [10] and [11] saw an antiline growing inside the PL dip when $B \perp E_{\text{las}}$. We think that the difference between our experiments come from the fact that we are using denser NV ensembles, and that any effects tied to the laser polarization are hidden by the stronger effects discussed previously.

1.3 NV-NV CR under purely transverse magnetic field

We now want to experimentally discriminate these different contributions and to see how close the actual decay rates are to the predicted ones.

One of the reason we want to separate these contributions is that they scale differently with the different variables of the sample (T_2^*, γ_f , magnetic VS electric noise ...). Understanding which of these effect dominates the zero field dynamics might give us insight on which parameter to optimize if one wants to avoid the zero field depolarization, or on the contrary to increase it.

The ideal way to isolate each contributions would be to apply an electric field strong enough to split the transition of the 4 classes, and to measure the decay rate of a single class dominated by the transverse electric field. Such an electric field would need to be of the order of $\sim 10^6$ V/cm, which is several order of magnitudes greater than the breakdown voltage of air and out of our experimental reach.

Instead of an electric field, we will use a transverse magnetic field, which as described in sec. 1.1.2 leads to a spin Hamiltonian similar to the one where the transverse electric field dominates, or at least to similar eigenstates.

1.3.1 Principle of the experiment

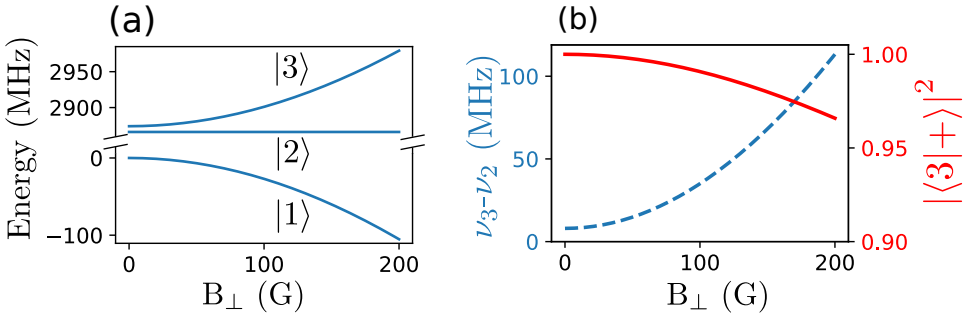

Figure 1.8: Simulation of the eigenstates of the NV Hamiltonian for $d_\perp E_p erp = 4$ MHz and a purely transverse magnetic field $B_\perp$. (a) Eigenvalues for the spin Hamiltonian as a function of $B_\perp$. The three states are labeled $|1\rangle$, $|2\rangle$ and $|3\rangle$ (b) Splitting between the $|2\rangle$ and $|3\rangle$ states (blue curve) and closeness factor $|\langle 3|+\rangle|^2$ between the $|3\rangle$ and $|+\rangle$ (red curve)

Fig. 1.8 shows a simulation of the eigenstates and eigenenergies for a NV Hamiltonian subject to transverse electric field and magnetic field. For convenience we chose to take $E_\perp = E_x$ and $B_\perp = B_x$, taking other geometric configuration only alters slightly the results. We labeled the eigenstates of the Hamiltonian $|1\rangle$, $|2\rangle$ and $|3\rangle$ in ascending order of energy.

Fig. 1.8-b) shows both the splitting $\Delta\nu$ between the $|2\rangle$ and $|3\rangle$ states, and how close the $|3\rangle$ state is to the $|+\rangle = \frac{|+1\rangle+|-1\rangle}{\sqrt{2}}$ state via the factor $|\langle 3|+\rangle|^2$. We look at the $|3\rangle$ state since $|2\rangle = |-\rangle = \frac{|+1\rangle-|-1\rangle}{\sqrt{2}}$ in this case.

These two metrics, $\Delta\nu$ and $|\langle 3|+\rangle|^2$ are what we are interested in: we want to increase $\Delta\nu$ to the point where the double flips are completely quenched, but we want $|\langle 3|+\rangle|^2$ to remain close to 1 since we wanted to observe the modification caused by the eigenbasis $\{|0\rangle, |\pm\rangle\}$. This way we can isolate the T_1^{dd} contribution coming from the change of eigenstates to the one coming from the double flips. Based on the plots in Fig.1.8-b), the region with $B_\perp \in [100,200]$ G seems to satisfy both these criteria.

1.3.2 Experimental data

We perform here a T_1^{dd} measurement similar to the one presented in Fig. [REF], on the same sample and with the same fitting parameters, but this time probing a class orthogonal to the magnetic field.

Fig. 1.9-a) and b) show the evolution of the transition frequencies $\nu_+ = \frac{E_{|3\rangle}-E_{|1\rangle}}{h}$ and $\nu_- = \frac{E_{|2\rangle}-E_{|1\rangle}}{h}$ where $|1\rangle$, $|2\rangle$ and $|3\rangle$ are the states described in Fig. 1.8. The magnetic field was scanned between 20 and 130 G by increment of ~ 0.5 G.

Fig. 1.9-c) shows the evolution of $1/T_1^{\text{dd}}$ with the magnetic field. We have denoted two region: in region A, $1/T_1^{\text{dd}}$ decreases with the magnetic field, from a value of 350 s^{-1} to a value of 185 s^{-1}. In region B, the value of $1/T_1^{\text{dd}}$ is stable and does not decrease further when $B_\perp$ or $\Delta\nu = \nu_+ = \nu_-$ are increased.

We attribute the decrease in region A to the double flips: as the magnetic field and $\Delta\nu$ are increased, the double flips become less and less resonant to the point where they become completely quenched for $B_\perp \approx 90$ G or $\Delta\nu \approx 30$ MHz. This value is coherent with the previously measured fluctuator linewidth. We can then estimate the part of the double flips in the low field (20 G here) depolarization rate and find that they amount for $\sim 50\%$ in this case.

Another possibility to explain this drop could be that the class orthogonal to $\mathbf{B}$ still exerts flip-flops with the other classes at low magnetic field, as we can see that they are not very far detuned in Fig. 1.9-a), but we have to consider that the detuning between the two states $\nu_+ - \nu_- = 9$ MHz is significantly lower, even at $B_\perp = 20$ G, than the detuning with the closest class $\nu_\pm - \nu_{\text{other}} = 22$ MHz; and also that there seem to be a small plateau for $1/T_1^{\text{dd}}$ at the beginning of region A, which is consistent with the double flip hypothesis since $\nu_+ - \nu_-$ is almost flat in this region while $\nu_\pm - \nu_{\text{other}}$ increases linearly with the magnetic field.

We now turn to region B. Even tough the double flips are completely quenched, the effects of the eigenbasis modification and the T_2^* reduction are

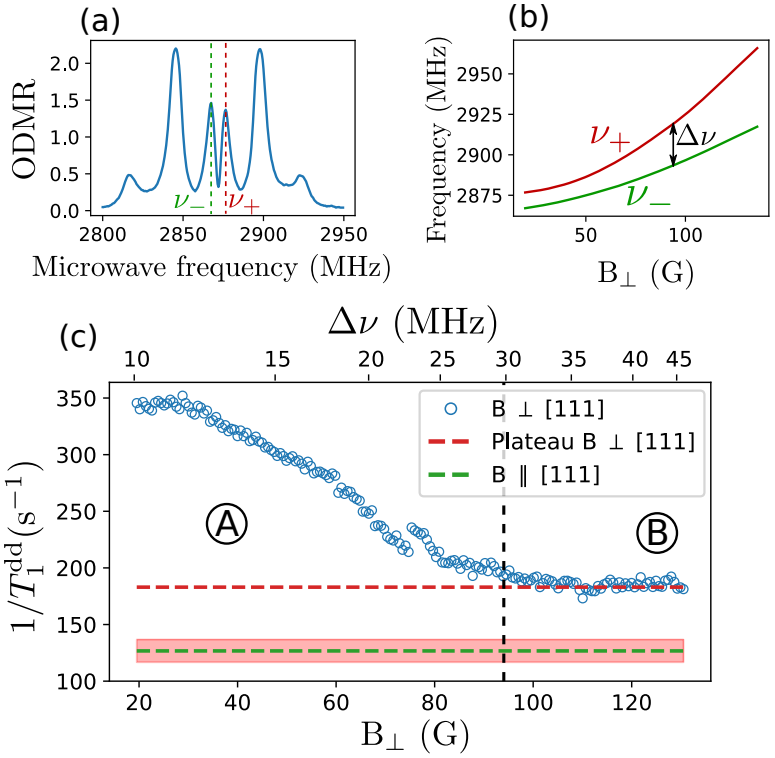

Figure 1.9: Experimental data for the depolarization under purely transverse magnetic field on sample ADM-150-2. a) ODMR spectrum for $|\mathbf{B}| = 20$ G. The transitions of the class orthogonal to the magnetic field are labeled ν_+ and ν_-. b) Dependency of ν_+ and ν_- with the magnetic field, as measured through ODMR. c) Measurement of T_1^{dd} as a function of the transverse magnetic field. The corresponding energy splittings $\Delta\nu = \nu_+ - \nu_-$ are written on top. We divided the plot between the A region where $1/T_1^{\text{dd}}$ decreases, and the B region where it reaches a plateau with a value $1/T_1^{\text{dd}} = 185 \pm 5$ s^{-1} indicated by a red line. We also indicate in green the value found for a purely longitudinal magnetic field $1/T_1^{\text{dd}} = 126 \pm 10$ s^{-1}

still present, because we can see on Fig. 1.8-b) that the eigenstates of the spin Hamiltonian are still very close to $\{|0\rangle, |\pm\rangle\}$ for these magnetic field values.

To evaluate the contribution of the eigenbasis and T_2^*, we measure the same class of NV centers, but this time with a longitudinal magnetic field ($B_\parallel \sim 100G$) to get a baseline value of $1/T_1^{\text{dd}}$ in the $|\pm1\rangle$ basis. We found a value of $1/T_1^{\text{dd}} = 126 \pm 10$ s^{-1} in this case, reported on Fig. 1.9-c) as a green line.

We do find that the decay rate is higher in the $|\pm\rangle$ basis by $\sim 50\%$ which corroborates our predictions, as both the change of eigenbasis from $|\pm1\rangle$ to

$|\pm\rangle$ and the increase of T_2^* in the $|\pm\rangle$ basis are predicted to increase the depolarization rate. The theoretical increase however overestimates once again the actual increase: for the change of eigenbasis alone we predicted an increase of the decay rate by a factor of 4 (see appendix [REF]), over 8 times more than the actual increase.

We unfortunately cannot experimentally discriminate the depolarization coming from the eigenbasis change or the T_2^* while using the same sample, since both of this properties are tied to the Hamiltonian eigenstates. But we do know that in this scenario, for a single isolated class, the contribution of both the change of eigenbasis and T_2^* amounts for ~ 3 times less than the double flips.

Based on these observation, we expect that difference in NV polarization between the $\mathbf{B} = 0$ region and $\mathbf{B} \neq 0$ region is caused by, in order of importance:

1. The lift of degeneracy between the four classes caused by the projection of the magnetic field on the different NV axis.

2. The double flips between the nearly resonant $|+\rangle$ and $|-\rangle$ states at low magnetic field.

3. The change of the Hamiltonian eigenbasis from $\{|0\rangle, |\pm\rangle\}$ in the electric field dominated region to $\{|0\rangle, |\pm 1\rangle\}$ in the magnetic field dominated region, and the incident change in T_2^*.

1.4 Introduction to ensemble NV magnetometry

Before we explore the application of low field depolarization to magnetometry, we must discuss the general field of NV magnetometry.

NV magnetometry is generally decomposed between single NV and ensemble magnetometry. Single NVs,often associated with scanning probes, offer a spatial resolution limited only by how far the magnetic source can be from the NV center (typically ~ 10 nm), but at the cost of a relatively low sensitivity (typically $\sim \mu\mathrm{T}/\sqrt{\mathrm{Hz}}$ [12]).

Ensemble NV centers center on the other hand offer sensitivities below 1 $\mathrm{pT}/\sqrt{\mathrm{Hz}}$ [13], at the cost of working working with samples of several hundreds of μm.

We will only focus here on NV ensemble magnetometry since we want to give elements of comparisons with our technique based on NV-NV CR. We will not try to give a complete overview of this field, but only to the elements close to the technique we present. For a general overview on microwave-based ensemble NV magnetometry, we recommend the excellent review from Barry et al [14].

1.4.1 AC and DC magnetometry

The most sensitive NV magnetometry protocols use the free precession of the spins to map a small change in the Zeeman energy into the phase of the spins, which is then converted in population. These protocols are generally distinguished between DC-broadband and AC-narrow band.

For DC-broadband magnetometry, the general technique consist of a Ramsey interferometry experiment, presented in chapter 1, which is limited by the spin inhomogeneous coherence time T_2^*. The bandwidth of the protocol is limited by the repetition rate of the experiment, generally up to $\sim$ 100 kHz. Although less sensitive in theory, continuous-wave (CW) ODMR and pulsed ODMR are also often employed for DC magnetometry. The state of the art in term of DC ensemble magnetometry is a sensitivity of $\sim 20pT/\sqrt{\text{Hz}}$ AC: pas oublier. J'ai oublié. Nan en vrai j'ai pas oublié, mais je le mettrai dans la partie sans uW

1.4.2 Low field magnetometry

Dans le dernier papier de Jelezko y'a des vrais raisons de faire du low field

1.4.3 Microwave-free magnetometry

Bubu et les russes

Orientation-free magnetometry

Arcizet

1.5 Low field depolarization magnetometry

1.5.1 Principle of the experiment

1.5.2 Characterization of the experiment

sensi, dépendence sensi angle, variance d'allan

1.5.3 Comparison with other magnetometry protocol

Budker : mesurer vite deuf les pentes

1.6 Conclusion and perspectives

- Improvement to the sensitivity : Scale up (les deux papiers sur le picoTesla mW, avec les deux systèmes), material optimization (15N !, [NV] concentration,)

- Understand the impact of the various factors on the flip-flop CR and DQ CR: T2*, strain, local electric noise ... Mettre ici les deux adamas du 20210927 avec le petit et le gros DQ, et peut etre aussi les DQ et SQ qui s'inversent sur le substrat. Comprendre

- Application for uneven surfaces, polycrystalline heteroepithaxy, low/no microwave environment (dimaond anvil cells, bio sensing).

Bibliography

[1] MW Doherty et al. "Theory of the ground-state spin of the NV- center in diamond". In: *Physical Review B* 85.20 (2012), p. 205203.

[2] Péter Udvarhelyi et al. "Spin-strain interaction in nitrogen-vacancy centers in diamond". In: *Physical Review B* 98.7 (2018), p. 075201.

[3] Thomas Mittiga et al. "Imaging the local charge environment of nitrogen-vacancy centers in diamond". In: *Physical review letters* 121.24 (2018), p. 246402.

[4] Eric Van Oort and Max Glasbeek. "Electric-field-induced modulation of spin echoes of NV centers in diamond". In: *Chemical Physics Letters* 168.6 (1990), pp. 529–532.

[5] Michael SJ Barson et al. "Nanomechanical sensing using spins in diamond". In: *Nano letters* 17.3 (2017), pp. 1496–1503.

[6] Ziwei Qiu et al. "Nuclear spin assisted magnetic field angle sensing". In: *npj Quantum Information* 7.1 (2021), pp. 1–7.

[7] Ziwei Qiu et al. "Nanoscale Electric Field Imaging with an Ambient Scanning Quantum Sensor Microscope". In: *arXiv preprint arXiv:2205.03952* (2022).

[8] P Jamonneau et al. "Competition between electric field and magnetic field noise in the decoherence of a single spin in diamond". In: *Physical Review B* 93.2 (2016), p. 024305.

[9] Benjamin Smeltzer, Jean McIntyre, and Lilian Childress. "Robust control of individual nuclear spins in diamond". In: *Physical Review A* 80.5 (2009), p. 050302.

[10] SV Anishchik et al. "Low-field feature in the magnetic spectra of NV- centers in diamond". In: *New Journal of Physics* 17.2 (2015), p. 023040.

[11] DS Filimonenko et al. "Weak magnetic field effects on the photoluminescence of an ensemble of NV centers in diamond: experiment and modelling". In: *Semiconductors* 54.12 (2020), pp. 1730–1733.

[12] Matthew Pelliccione et al. “Scanned probe imaging of nanoscale magnetism at cryogenic temperatures with a single-spin quantum sensor”. In: *Nature nanotechnology* 11.8 (2016), pp. 700–705.

[13] Thomas Wolf et al. “Subpicotesla diamond magnetometry”. In: *Physical Review X* 5.4 (2015), p. 041001.

[14] John F Barry et al. “Sensitivity optimization for NV-diamond magnetometry”. In: *Reviews of Modern Physics* 92.1 (2020), p. 015004.